

# Experimental identification and validation of models in micro and macro plasticity

T. Hoffmann, J. Kalisch, A. Bertram, S. Shim, J. Z. Tischler, H. Bei, B. C. Larson

*For micro-macro approaches to finite plasticity, one needs experimental results on both scales, the engineering scale (macro scale) and the crystal scale (micro scale). Since we know that a monocrystal behaves different from a crystallite embedded in a polycrystal, one is also interested in data obtained on the micro scale of a polycrystal. Such data is needed not only for the identification of the material parameters like hardening variables, but also for the validation of these models. In this paper, experiments on both scales and, in parallel, FEM-simulations are presented, in order to compare the results of both approaches. The specimens stem from a rolled sheet of the deep-drawing steel DC04. On the micro scale indenter tests have been performed and the orientation changes in the volume below the indent have been measured using micron-resolution 3D x-ray microscopy (Larson et al., 2004, 2008). On the macro scale the usual tension tests and additional shear tests in different directions (Bouvier et al., 2006) have been performed. In corresponding simulations, the micro-macro transition is performed by a full constrained Taylor-model and, in order to overcome the drawbacks of the Taylor-model, the RVE technique has been applied.*

## 1 Introduction

Micro-macro approaches are of increasing importance for metal forming simulations (Habraken, 2004) and, accordingly, the number of new micro-macro models increases too. Thus a need of adequate identification and validation tests arises for such models. Usually the identification and validation is exclusively done on the macro scale with the advantage to apply well established experimental techniques. In former publications this procedure led to conclusive results, but with an increasing complexity of the models, also the number of parameters increases. For this reason the information content of classical experimental data is not sufficient anymore and a definite identification becomes more problematic. There are two possibilities to enhance the amount of experimental information. On the one hand a higher variety of experiments can be used. On the other hand the variety of experimental observed data can be raised. These two possibilities will be discussed in the following.

In the case of sheet metals several macroscopic experiments have been reviewed by Kuwabara (2007). However, beside new macroscopic experiments the use of single-crystal experiments has been suggested as well. Here one has to differentiate between monolithic single-crystals directly grown from the melt, and single-crystals within a polycrystal. Since the monolithic single-crystal behaves different from the single-crystal within a polycrystal, the use of monolithic single-crystals is not adequate if the identification and validation scheme incorporates micro- and macro-experiments. Fortunately, the progress in miniaturisation offers the possibility to apply experiments on a single grain within a polycrystal like, e.g., microindentation or micro-compression tests. Data from these experiments can be directly compared with data calculated by the micro-models. Since the focus of this paper is set on the validation of a crystal plasticity model by the use of microindentation tests, the following discussion follows similar lines. Liu et al. (2005) performed nanoindentation tests in single crystal copper. They calibrated the hardening parameters of their crystal plasticity model by means of the load-displacement curve. In the work of Casals et al. (2007) pyramidal nano-indentation into a single grain of polycrystalline copper has been performed. They have validated their model by a comparison of experimental and calculated load-displacement curves. The material parameters used have been previously identified by a tensile test of monolithic single-crystal copper.

As already mentioned before an improvement of the identification and validation procedure can also be reached by an increase of the variety of experimental data. On the macro scale Kreißig (1998) presented an identification procedure for a macroscopic elasto-plastic material model by the use of displacement field data. In the case of micro scale indentation experiments, two possible kinds of field data can be measured. These are the out-of-plane

displacement of the indented surface (pile-up, sink-in) and the lattice orientations in the volume below the indentation dip. A comparison between measured and calculated surface displacements in the vicinity of an indentation dip has been done by Wang et al. (2004); Liu et al. (2005, 2008); Zambaldi et al. (2007) and Alcalá et al. (2008). Thus, Liu et al. (2008) have been able to adjust the friction coefficient of the used friction model. Furthermore Alcalá et al. (2008) found that the surface displacements are governed by the hardening description of the applied crystal plasticity model. This indicates the applicability of surface displacement data for identification and validation procedures. A comparison of measured and calculated lattice rotations has been performed by Zaafarani et al. (2006, 2008). They applied nano-indentation experiment on single-crystal copper, using a conical indenter with a spherical tip. An electron backscattered diffraction technic in combination with serial sectioning has been used to obtain the experimental data. They achieved a reasonable accordance between the rather large measured and calculated lattice rotations associated with a relatively deep penetration of a small tip-radius indenter.

Within this work we present a comprehensive identification and validation procedure on two scales. The experiments have been applied on DC04, a cold rolled deep drawing steel. As a material model a standard crystal plasticity model (Bertram, 2008) is used. Non-Schmid effects have been neglected in the current context. While the hardening parameters have been identified by macro scale shear tests, the validation of these parameters is performed by comparing simulations of macro scale tensile tests and micro scale indentation tests. The micro-indentation tests have been applied on single grains of the rolled sheet. The lattice rotations in the volume below the indent have been measured using micron-resolution 3D x-ray microscopy (Yang et al., 2004a,b; Larson et al., 2004, 2008). In contrast to the EBSD based method, this technique can be applied without a previous sectioning of the indented material and thus the experimental data obtained by this technique are very suitable for comparing with the calculated data.

## 2 The sample material

The DC04 is a cold-rolled low carbon steel, typically used for deep drawing applications. Its chemical composition is shown in Table 1. All specimens stem from a sheet with a thickness of 0.8 mm, the microstructure of which is shown in Figure 1. The grains exhibit a relatively small morphological texture with a mean grain size of 19 and 13 microns in rolling and transversal direction, respectively. The crystallographic texture has been measured by

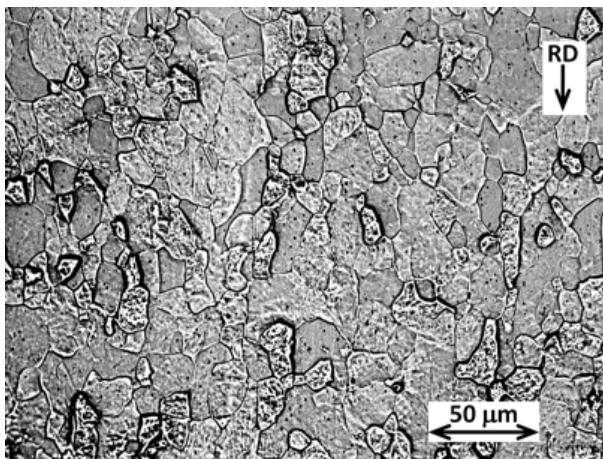


Figure 1: Microstructure of a DC04 steel sheet with 0.8 mm thickness

Table 1: Chemical composition of DC04

Element	C	Si	Mn	P	S	Al
max. wt%	0.08	-	0.4	0.03	0.03	-

a neutron diffraction method. The resulting pole figures in Figure 2 indicate a strong rolling texture. These pole figures are approximated by a set of 2000 orientations (Figure 2).

## 3 Mechanical tests

Three different kinds of tests have been applied, namely shear and tensile tests on the macro scale, and indentation tests on the micro scale. All tests have been applied at room temperature and in a quasistatic regime. Thus temperature and inertial effects are negligible.

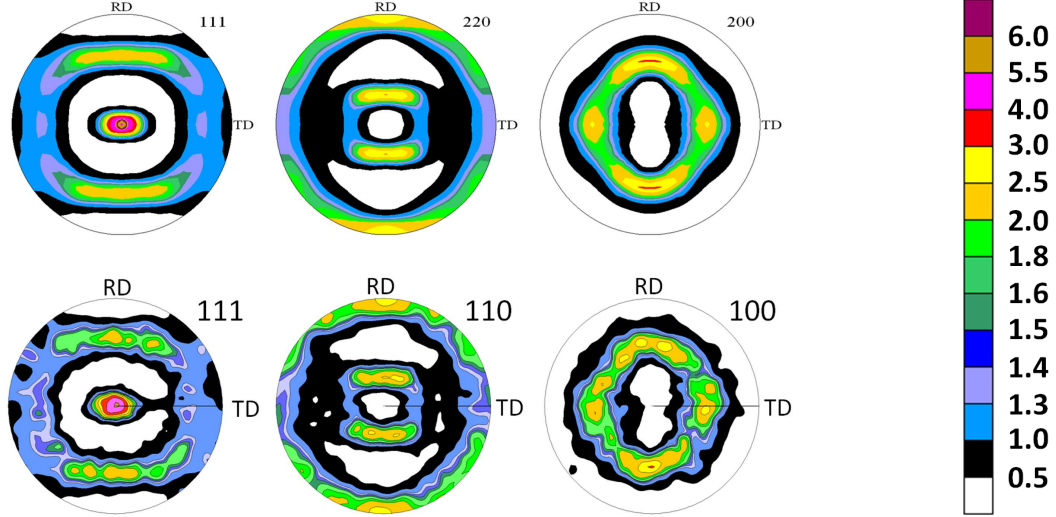


Figure 2: Measured (upper row) and approximated (lower row) pole figures

### 3.1 Macroscopic shear test

Monotonic shear tests in seven different directions ( $0^\circ$ ,  $15^\circ$ ,  $30^\circ$ ,  $45^\circ$ ,  $60^\circ$ ,  $75^\circ$ ,  $90^\circ$ ) with respect to the rolling direction have been performed. These deformation controlled tests have been carried out with a shear rate of  $1.8 \cdot 10^{-3} s^{-1}$ . The shear region of the test specimens are  $30 \text{ mm}$  in length and  $3 \text{ mm}$  in width. A precise description of the shear tests can be found in Bouvier et al. (2006).

### 3.2 Macroscopic tensile test

Tensile tests in three different directions with respect to the rolling direction ( $0^\circ$ ,  $45^\circ$ ,  $90^\circ$ ) have been performed using specimens with a length of  $80 \text{ mm}$  and a width of  $20 \text{ mm}$ . All test have been conducted with a strain-rate of  $2.5 \cdot 10^{-3} s^{-1}$ , and during the tests, the tensile force and the change in length and width are continuously measured. From these data the stress-strain curves and the  $r$ -values (Lankford-coefficients) have been obtained. The  $r$ -values are calculated by

$$r = \frac{\ln\left(\frac{b_0}{b}\right)}{\ln\left(\frac{lb}{l_0 b_0}\right)} \quad (1)$$

with  $l$  and  $b$  being the current and  $l_0$  and  $b_0$  the initial length and width, respectively. Since the experimental measured  $r$ -values do not show a significant strain-dependence, this classical definition of the  $r$ -values is sufficient.

### 3.3 Microscopic indentation test

With the help of microindentation tests it is possible to investigate the single-crystal behaviour of a grain within a polycrystal. Therefore, spherical indentation has been applied to single grains of the rolled sheet. However, to achieve single-crystal behavior within a particular grain it is necessary that the indentation be performed sufficiently distant from the grain boundaries, which is not possible with the DC04 grain size shown in Figure 1. In order to fulfill this condition, a larger grain size of  $\sim 100 \mu\text{m}$  was achieved by annealing DC04 samples for microindentation for  $18 \text{ hr}$  at  $1200^\circ \text{ C}$ . Microindentation was conducted at room temperature with a spherical sapphire indenter of  $100 \mu\text{m}$  radius. Two different loading procedures have been used in the tests. While in a first series of tests the loading,  $P$ , was applied with a constant loading rate  $\frac{\partial P}{\partial t} = 1 \text{ mNs}^{-1}$ , the second series was performed in the continuous stiffness mode (CSM) with a constant fractional loading rate of  $\frac{\partial P}{\partial t} P^{-1} = 0.05 s^{-1}$  up to a maximum load of  $500 \text{ mN}$ . For DC04 steel, this resulted in different indentation tip velocities which can be derived from the slopes of the time-displacement data shown in Figure 4. In addition to measuring the indentation load-displacement curves, ex situ, micron resolution, 3D x-ray microscopy measurements of the local lattice rotations in the indented material were performed on the Sector 34 ID-E microbeam facility at the Advanced Photon

Source at Argonne National Laboratory. The 3D x-ray microscopy measurements were performed as described previously (Yang et al., 2004a,b; Larson et al., 2008) using a  $\sim 0.5 \mu m$  diameter polychromatic microbeam and an area detector providing angular orientation determinations with  $\sim 0.01$  degree angular precision. The rotational deformation measurements were made on a plane perpendicular to the sample surface passing through the middle of the indentation by sequential line scan measurements (to depths of  $\sim 40 \mu m$  below the sample surface) with one micron translation of the sample between scans.

## 4 Numerical model

### 4.1 Material model

The material behaviour is modeled by a standard single-crystal elastic-viscoplastic model, which is based on the concept of isomorphic elastic ranges (Bertram, 2008). Herein the plastic transformation  $\mathbf{P}$  describes the change of lattice vectors in the elastic law due to slip. In the following formulas the tilde ( $\sim$ ) marks all values which are described with respect to the initially undisturbed lattice base. For a given strain state in terms of the Green strain tensor  $\tilde{\mathbf{E}}^G$ , the 2. Piola-Kirchhoff stress tensor

$$\tilde{\mathbf{T}}^{2PK} = \tilde{\mathbb{K}}[\tilde{\mathbf{E}}^G] \quad \text{with} \quad \tilde{\mathbf{E}}^G = \frac{1}{2}(\tilde{\mathbf{C}} - \mathbf{I}), \quad \tilde{\mathbf{C}} = \mathbf{P}^T \mathbf{F}^T \mathbf{F} \mathbf{P} \quad (2)$$

is calculated by the use of an anisotropic linear elastic law. In Eq. 2,  $\mathbf{F}$  is the deformation gradient and  $\tilde{\mathbb{K}}$  is the stiffness tetrad for a cubic crystal. The tetrad contains three independent elastic constants which have been assumed to be those of pure iron. This assumption is justified because of the low carbon content of the DC04. At room temperature the sample material shows a bcc crystal structure. We assume crystallographic slip on the commonly used  $\{110\}\langle 111 \rangle$  and  $\{112\}\langle 111 \rangle$  slip systems. These 24 slip systems are described by the Schmid-tensor which is the dyadic product of slip direction  $\tilde{\mathbf{d}}_\alpha$  and slip plane normal  $\tilde{\mathbf{n}}^\alpha$ . Slip occurs if the resolved shear stress

$$\tau^\alpha = \tilde{\mathbf{C}} \tilde{\mathbf{T}}^{2PK} \cdot (\tilde{\mathbf{d}}_\alpha \otimes \tilde{\mathbf{n}}^\alpha) \quad . \quad (3)$$

in a slip system  $\alpha$  reaches a critical value. The resulting shear-rates are calculated by the viscous ansatz of Hutchinson (1976)

$$\dot{\gamma}^\alpha = \dot{\gamma}_0 \operatorname{sgn}(\tau^\alpha) \left| \frac{\tau^\alpha}{\tau_c} \right|^{\frac{1}{m}} \quad . \quad (4)$$

Within this ansatz two additional material parameters are needed. Hutchinson already stated that  $\dot{\gamma}_0$  can be selected arbitrarily without loss of generality. The second parameter, the strain-rate sensitivity  $m$ , strongly depends on temperature and strain-rate itself. It can be derived from strain-rate experiments. A comprehensive representation of strain rate experiments for a polycrystalline mild steel ES is given by Rusinek et al. (2007). Because of the similar chemical composition of DC04 and mild steel ES we have adopted the strain-rate sensitivity from Rusinek et al. (2007). For the introduced model the microscopic strain-rate sensitivity is equal to the macroscopic one. The critical resolved shear stress is described by

$$\tau_c = \tau_{c0} + (\tau_s - \tau_{c0}) \left( 1 - \exp\left(\frac{-\theta_0 \gamma}{\tau_s}\right) \right) + \theta_\infty \gamma \quad \text{with} \quad \gamma = \int \sum_\alpha |\dot{\gamma}_\alpha| dt \quad . \quad (5)$$

This function is based on an approach proposed by Kocks (1976). The original approach, which regards stage II and III hardening, has been extended by a linear term with  $\theta_\infty$ . With this additional term a saturation of the critical resolved shear stress is avoided, which can be interpreted as stage IV hardening. For the hardening rule 4 material parameters are needed, namely the initial critical resolved shear stress  $\tau_{c0}$ , a saturation stress  $\tau_s$ , an initial hardening modulus  $\theta_0$  and a remaining hardening modulus  $\theta_\infty$ . The flow rule

$$\mathbf{P}^{-1} \dot{\mathbf{P}} = - \sum_\alpha \dot{\gamma}_\alpha (\tilde{\mathbf{d}}_\alpha \otimes \tilde{\mathbf{n}}^\alpha) \quad (6)$$

describes the evolution of the plastic transformation (Bertram, 2008). This model has been implemented in a user subroutine (UMAT) of the finite element code ABAQUS. The discretisation is done by means of a backward Euler scheme (Böhleke et al., 2006).

## 4.2 Micro-macro transition

In most calculations of this work a fully constrained Taylor-model is used. Within this model a homogeneous strain distribution is assumed. However, in some cases also the RVE-technique was used for comparison. The RVE consists of 8000 linear fully integrated hexahedral elements. Within the RVE the grain shapes are not taken into consideration, due to the fact, that the polycrystal behaviour is influenced by the crystallographic rather than by the morphological texture. This means that every element represents one grain. Periodic displacement boundary conditions have been applied. For both models the macroscopic stresses and strains are the volume average of the microscopic one.

## 4.3 Micro scale FEM model

The FEM-model for the microindentation test consists of two parts, a specimen which represents the grain, and the indenter. The specimen mesh which has been refined in the contact zone, is shown in Figure 3. It consists of 22000 linear fully integrated hexahedral elements. The whole specimen is modelled as a single-crystal with the orientation of the particular indented grain. On the bottom zero displacement boundary conditions and on the sides stress free boundary conditions have been applied. In order to reduce computational costs the indenter is modelled as a rigid sphere which can be solely controlled by displacement boundary conditions. Since the experiments have been performed in a load controlled manner, the measured time-displacement data have been used to control the simulations (see Figure 4). The contact interaction between indenter and specimen is implemented by the standard

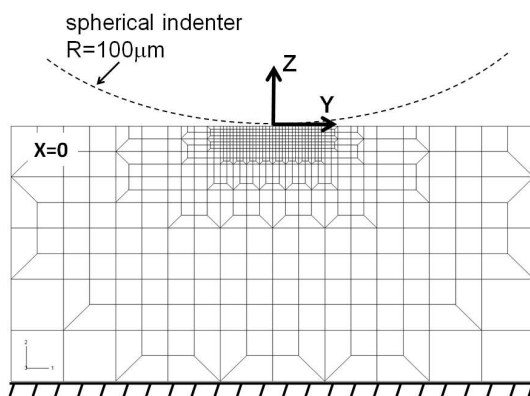


Figure 3: FEM mesh cross section and sample coordinate system

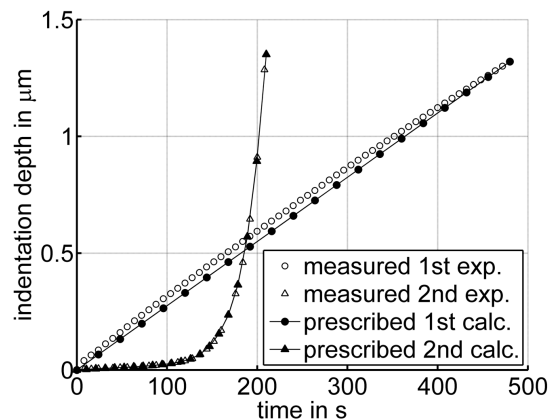


Figure 4: Measured indentation depths with respect to the testing time for both tests and the corresponding simulation input data

Abaqus contact algorithms. The simulation of the indentation includes the orientation changes at all calculation points. For comparison with the experimental results it is convenient to represent this orientation change with respect to the coordinate axes in Figure 3, as calculated by a simple vector decomposition of the Euler-Rodrigues vector (Brannon, 2002).

## 5 Identification on the macro scale

The hardening parameters are identified by the use of the shear test in rolling direction. This inverse problem leads to a nonlinear minimisation problem and has been solved by the freeware package Minpack (Moré et al., 1984) using the Levenberg-Marquardt algorithm. In Figure 5 the measured and calculated shear stress with respect to the shear number are shown. However, the correctness of the identification is not guaranteed by this good agreement of both curves. An indication of possible errors can be derived from the correlation matrix (Kreißig et al., 2001). A numerical approximation of this matrix is given in Press et al. (1997). This matrix quantifies the correlation between the parameters which have been identified. If one off-diagonal element is  $\pm 1$  or if every off-diagonal element exceeds an absolute value of 0.9, the parameters are highly correlated and tend to be inaccurate (Beck and Arnold, 1977). With respect to these criteria, the correlation matrix (Table 2) derived for this identification is

acceptable. In Table 3 all assumed and identified material parameters are listed.

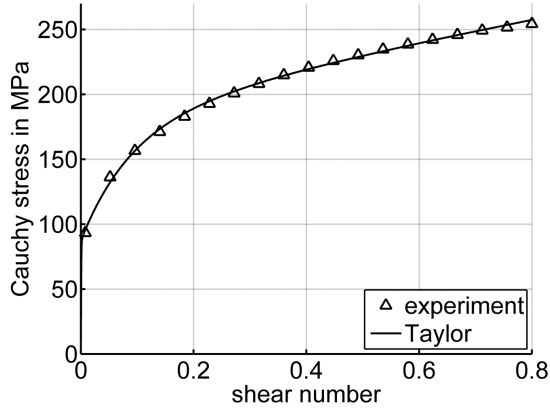


Table 2: Correlation matrix

	$\tau_{c0}$	$\tau_{cs}$	$\theta_0$	$\theta_\infty$
$\tau_{c0}$	1.00	0.38	-0.70	-0.34
$\tau_{cs}$		1.00	-0.77	-0.98
$\theta_0$	<i>Sym.</i>		1.00	0.71
$\theta_\infty$				1.00

Figure 5: Result of the curve fit for the shear test in rolling direction ( $0^\circ$ )

Table 3: Material parameters for DC04

$\tilde{K}_{1111}$	$\tilde{K}_{1122}$	$\tilde{K}_{1212}$	$\dot{\gamma}_0$	$m$	$\tau_{c0}$	$\tau_s$	$\theta_0$	$\theta_\infty$
231 GPa	135 GPa	116 GPa	$0.001 \text{ s}^{-1}$	0.02	57 MPa	115 MPa	804 MPa	43 MPa

## 6 Validation

### 6.1 Validation on the macro scale

A validation of the model is achieved, if the numerically predicted data is qualitatively and quantitatively similar to experimental data obtained from additional experiments. In the case of tensile tests two data sets, stress-strain curves and r-values can be compared. While the stress-strain curve is considered to be a validation for the hardening parameters, the r-values rather tend to be a validation for the homogenisation method and the initial texture. The stress-strain curves are fairly well predicted by the Taylor-model (Figure 6). However, the drawback of the Taylor-model becomes observable in the r-value prediction. Here RVE calculations have been applied to check the influence of the homogenisation method (Figure 7).

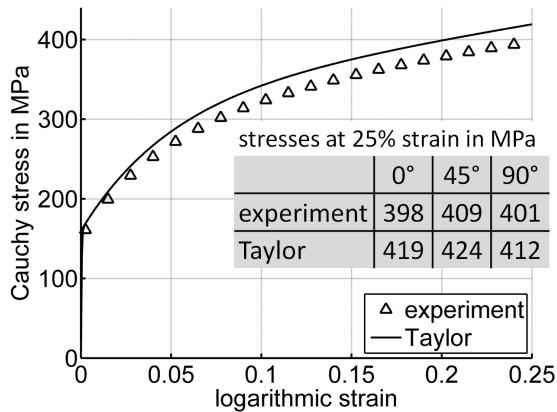


Figure 6: Predicted and measured stress-strain curves for the tensile test in rolling direction ( $0^\circ$ )

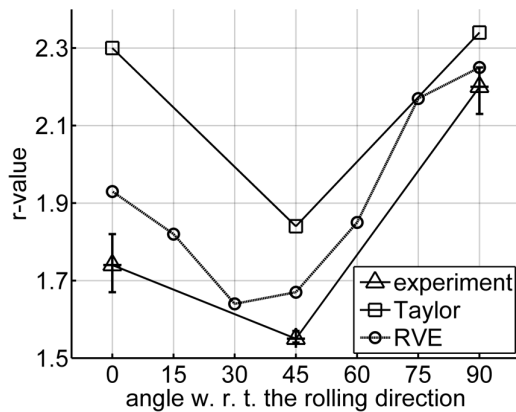


Figure 7: Experimental and predicted r-values over the specimen orientation

## 6.2 Validation on the micro scale

The material parameters which have been identified and validated on the macro scale are now used to predict the material behaviour on the micro scale. In this Section the measured and calculated data are compared for two different microindentation tests. The data consist of the lattice rotations below the indentation dip and the load-displacement curves. In Table 4 the initial orientations of the indented grains are shown. The lattice rotations

Table 4: Orientations of the indented grains with respect to the sample coordinate system (see Figure 3)

directions of the sample coordinate system	crystallographic directions first experiment	crystallographic directions second experiment
X	(-6.29, 1.00, 6.41)	( 3.71, -1.00, 2.86)
Y	( 1.00, -5.14, 1.78)	(-1.00, 3.49, 2.52)
Z	( 1.97, 1.00, 1.78)	(-1.05, -1.02, 1.00)

were measured in the  $(0, Y, Z)$  plane of the specimen, which is orthogonal to the surface and contains the center point of the indentation dip. For comparison between the measurements and calculations in this initial report, only the rotations around the x-axis (see Figure 3) are presented. The measured and calculated lattice rotations for both tests are shown as false-color contour plots in Figures 8 and 9. Good overall agreement can be seen between the measured and calculated rotation contours for both indentation tests without including the  $\sim 100 \mu\text{m}$  polycrystalline grain size of the sample. Moreover, comparison of the load displacement curves reveals good

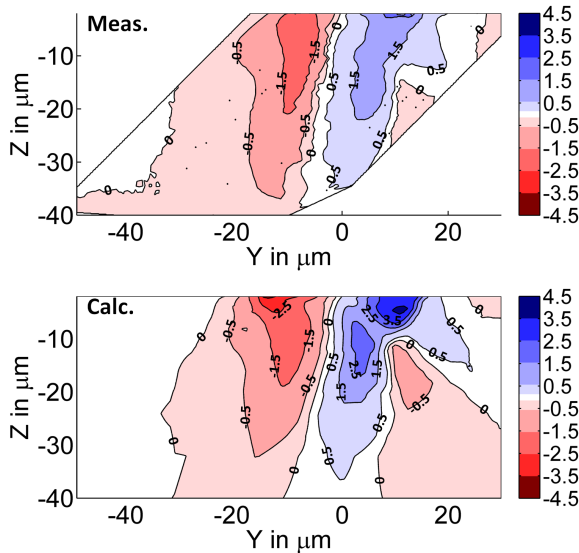


Figure 8: Measured (top) and calculated (bottom) lattice rotation around the x-axis (in degree), first experiment

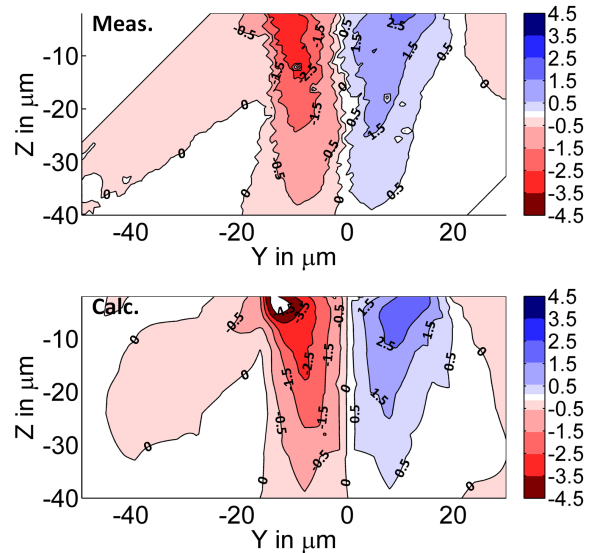


Figure 9: Measured (top) and calculated (bottom) lattice rotation around the x-axis (in degree), second experiment

agreement between experiment and simulation (Figures 10 and 11) as well. These results suggest that the grain boundaries were sufficiently distant from the indentation that near single crystal behavior is achieved and also that the influence of the anneal-induced coarsening of the grains on the mechanical properties is not too strong in these cases. We note that softening of the material by annealing would be expected to lead to an overestimation of the load-displacement curves in Figures 10 and 11, which is observed to some extent. Another issue is the influence of the homogenization method on the identification of hardening parameters for the calculations. The use of the RVE instead of the Taylor-model would be expected to result in higher hardening parameters and, subsequently, to calculated load-displacement curves showing a slightly stiffer behavior. With respect to the local lattice rotations, it can be seen that for the larger ( $> 1.5$  degrees) positive and negative rotations near the indent surfaces the calculations tend to overestimate the magnitude of the rotations somewhat. While these issues need to be investigated in detail taking the polycrystalline nature of the sample and the influence of surrounding grains into account directly, the correspondence between simulated and measured indent load-displacement curves and local lattice rotations is encouraging at this point. Although the indentations in this study are at much lower deformation levels, larger indentation tip radii, and larger length scales than the electron backscattering diffraction

investigations of Zaaferani et al. (2006, 2008), there are strong similarities in the correspondence between the measured and simulated deformation results. A more detailed discussion of the results, especially in the case of the lattice rotations, will be given in a forthcoming publication.

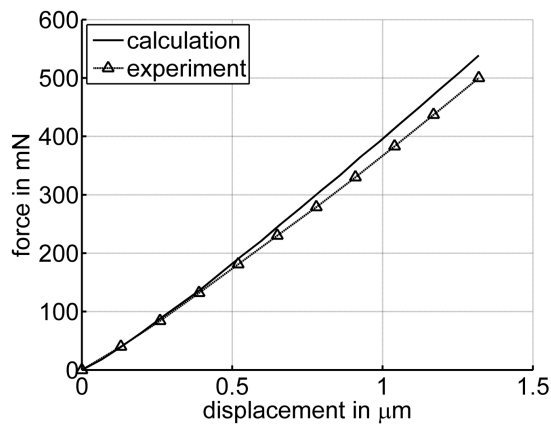


Figure 10: Measured and calculated load-displacement curve, first experiment

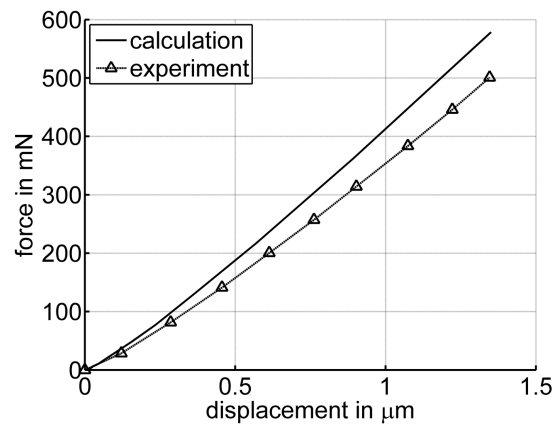


Figure 11: Measured and calculated load-displacement curve, second experiment

## 7 Conclusions

For a low carbon steel the hardening parameters of a standard crystal plasticity model have been identified and validated by the use of macroscopic shear and tensile tests. The model has been applied subsequently for simulations of spherical microindentation tests on single grains of a rolled sheet. In addition to the usual indentation load-displacement curves, simulations and 3D x-ray microscopy measurements of two-dimensional fields of lattice rotations have been compared. In this work we have demonstrated the possibility of linking calculations on macro and micro scales. While the calculated macro scale results are satisfying, room for improvement exists on the micro scale. Especially for the case of bcc materials, current discussions regarding the dominant micro-mechanisms exists (Seeger, 2004; Yalcinkaya et al., 2008) and the development of enhanced crystal plasticity models is in progress. The combination of methods outlined here opens the possibility to validate various micro-macro models on both scales. However, to identify material parameters on the micro scale and subsequently use those to predict the macroscopic material behaviour remains a future prospect, but the good agreement between the measured and calculated micro scale data presented here encourages further investigations in this direction.

## Acknowledgements

The financial support provided by the German Science Foundation (DFG) through GK 828 graduate school is sincerely acknowledged. Research at ORNL supported by the U. S. Department of Energy, Basic Energy Sciences, Division of Materials Sciences and Engineering; the Advanced Photon Source is supported by the U. S. DOE Division of User Facilities; S. Shim and H. Bei performed the indentations. We sincerely thank H.-G. Brokmeier (GKSS Geesthacht, Germany) for measuring the pole figures and W. Skrotzki (Technical Univ. Dresden, Germany) for the pole figure approximation. The tensile test data have been kindly provided by the InPro (Berlin, Germany). The shear tests have been supported by S. Bouvier (LPMTM-CNRS, Univ. Paris 13, France). M. Heilmaier (Technical Univ. Darmstadt, Germany) performed the heat treatment.

## References

- Alcalá, J.; Casals, O.; Ocenásek, J.: Micromechanics of pyramidal indentation in fcc metals: Single crystal plasticity finite element analysis. *J. Mech. Phys. Solids*, 56, (2008), 3277–3303.
- Beck, J. V.; Arnold, K. J.: *Parameter Estimation in Engineering and Science*. John Wiley and Sons (1977).
- Bertram, A.: *Elasticity and Plasticity of Large Deformations*. Springer-Verlag, 1st edn. (2005), 2nd edn. (2008).

- Böhlke, T.; Risy, G.; Bertram, A.: Finite element simulation of metal forming operations with texture based material models. *Modell. Simul. Mater. Sci. Eng.*, 14, (2006), 365–387.
- Bouvier, S.; Haddadi, H.; Levée, P.; Teodosiu, C.: Simple shear tests: Experimental techniques and characterization of the plastic anisotropy of rolled sheets at large strains. *J. Mater. Process. Technol.*, 172, (2006), 96–103.
- Brannon, R. M.: *A review of useful theorems involving proper orthogonal matrices referenced to three dimensional physical space.* [www.mech.utah.edu/~brannon/public/rotation.pdf](http://www.mech.utah.edu/~brannon/public/rotation.pdf) (2002).
- Casals, O.; Ocenásek, J.; Alcalá, J.: Crystal plasticity finite element simulations of pyramidal indentation in copper single crystals. *Acta Mater.*, 55, (2007), 55–68.
- Habraken, A. M.: Modelling plastic anisotropy of metals. *Arch. Comput. Meth. Eng.*, 11, 1, (2004), 3–96.
- Hutchinson, J. W.: Bounds and self-consistent estimates for creep of polycrystalline materials. *Proc. R. Soc. London, Ser. A*, 348, 1652, (1976), 101–127.
- Kocks, U. F.: Laws for work-hardening and low-temperature creep. *J. Eng. Mater. Technol.*, 98, 1, (1976), 76–85.
- Kreißig, R.: Auswertung inhomogener Verschiebungsfelder zur Identifikation der Parameter elastisch-plastischer Deformationsgesetze. *Forsch. Ingenieurswes.*, 64, (1998), 99–109.
- Kreißig, R.; Benedix, U.; Görke, U.-J.: Statistical aspects of the identification of material parameters for elastoplastic models. *Arch. Appl. Mech.*, 71, (2001), 123–134.
- Kuwabara, T.: Advances in experiments on metal sheets and tubes in support of constitutive modeling and forming simulations. *Int. J. Plast.*, 23, 3, (2007), 385–419.
- Larson, B. C.; Tischler, J. Z.; El-Azab, A.; Liu, W.: Dislocation density tensor characterization of deformation using 3D X-ray microscopy. *J. Eng. Mater. Technol.*, 130, 2, (2008), 0210241–02102410.
- Larson, B. C.; Yang, W.; Tischler, J. Z.; Ice, G. E.; Budai, J. D.; Liu, W.; Weiland, H.: Micron-resolution 3-D measurement of local orientations near a grain-boundary in plane-strained aluminium using X-ray microbeams. *Int. J. Plast.*, 20, 3, (2004), 543–560.
- Liu, Y.; Varghese, S.; Ma, J.; Yoshino, M.; Lu, H.; Komanduri, R.: Orientation effects in nanoindentation of single crystal copper. *Int. J. Plast.*, 24, (2008), 1990–2015.
- Liu, Y.; Wang, B.; Yoshino, M.; Roy, S.; Lu, H.; Komanduri, R.: Combined numerical simulation and nanoindentation for determining mechanical properties of single crystal copper at mesoscale. *J. Mech. Phys. Solids*, 53, (2005), 2718–2741.
- Moré, J. J.; Sorensen, D. C.; Hillstrom, K. E.; Garbow, B. S.: The minpack project. In: W. J. Cowell, ed., *Sources and Development of Mathematical Software*, pages 88–111, Prentice-Hall (1984).
- Press, W. H.; Teukolsky, S. A.; Vetterling, W. T.; Flannery, B. P.: *Numerical recipes in Fortran 77.* Cambridge University Press (1997).
- Rusinek, A.; Zaera, R.; Klepaczko, J. R.: Constitutive relations in 3-D for a wide range of strain rates and temperatures - Application to mild steels. *Int. J. Solids Struct.*, 44, (2007), 5611–5634.
- Seeger, A.: Experimental evidence for the  $\{110\} \leftrightarrow \{112\}$  transformation of the screw-dislocation cores in body-centred cubic metals. *Phys. Stat. Sol.*, 201, 4, (2004), R21–R24.
- Wang, Y.; Raabe, D.; Klüber, C.; Roters, F.: Orientation dependence of nanoindentation pile-up patterns and of nanoindentation microtextures in copper single crystals. *Acta Mater.*, 52, (2004), 2229–2238.
- Yalcinkaya, T.; Brekelmans, W. A. M.; Geers, M. G. D.: BCC single crystal plasticity modeling and its experimental identification. *Modell. Simul. Mater. Sci. Eng.*, 16(8), (2008), 085007.
- Yang, W.; Larson, B. C.; Pharr, G. M.; Ice, G. E.; Budai, J. D.; Tischler, J. Z.; Liu, W.: Deformation Microstructure Under Microindents in Single-Crystal Cu Using Three-Dimensional X-Ray Structural Microscopy. *J. Mater. Res.*, 19, 1, (2004a), 66–72.
- Yang, W.; Larson, B. C.; Tischler, J. Z.; Ice, G. E.; Budai, J. D.; Liu, W.: Differential-Aperture X-Ray Structural Microscopy: A Submicron-Resolution Three-Dimensional Probe of Local Microstructure and Strain. *Micron*, 35, 6, (2004b), 431–439.

Zaafarani, N.; Raabe, D.; Roters, F.; Zaefferer, S.: On the origin of deformation-induced rotation patterns below nanoindents. *Acta Mater.*, 56, (2008), 31–42.

Zaafarani, N.; Raabe, D.; Singh, R. N.; Roters, F.; Zaefferer, S.: Three-dimensional investigation of the texture and microstructure below a nanoindent in a Cu single crystal using 3D EBSD and crystal plasticity finite element simulations. *Acta Mater.*, 54, (2006), 1863–1876.

Zambaldi, N.; Roters, F.; Raabe, D.; Glatzel, U.: Modeling and experiments on the indentation deformation and recrystallization of a single-crystal nickel-base superalloy. *Mater. Sci. Eng., A*, 454-455, (2007), 433–440.

---

*Addresses:* T. Hoffmann, J. Kalisch, A. Bertram, Otto-von-Guericke University, Institut for Mechanics, Universitaetsplatz 2, 39106 Magdeburg, Germany. S. Shim, Research Institute of Industrial Science and Technology, Gyunggi 445-813, Korea. J. Z. Tischler, H. Bei, B. C. Larson, Materials Science & Tech. Div. Oak Ridge Nat. Lab., Oak Ridge, TN37831, USA.

email: albrecht.bertram@ovgu.de    laronbc@ornl.gov